J. Anat. (2005) **207**, pp135–144

Development of sensory innervation in rat tibia: co-localization of CGRP and substance P with growth-associated protein 43 (GAP-43)

Mariusz Gajda,[1] Jan A. Litwin,[1] Tadeusz Cichocki,[1] Jean-Pierre Timmermans[2] and Dirk Adriaensen[2]

[1]*Department of Histology, Jagiellonian University, Medical College, Kraków, Poland*
[2]*Laboratory of Cell Biology and Histology, Department of Biomedical Sciences, University of Antwerp, Belgium*

Abstract

The development of sensory innervation in long bones was investigated in rat tibia in fetuses on gestational days (GD) 16–21 and in neonates and juvenile individuals on postnatal days (PD) 1–28. A double immunostaining method was applied to study the co-localization of the neuronal growth marker growth-associated protein 43 (GAP-43) and the pan-neuronal marker protein gene product 9.5 (PGP 9.5) as well as that of two sensory fibre-associated neuropeptides, calcitonin gene-related peptide (CGRP) and substance P (SP). The earliest, not yet chemically coded, nerve fibres were observed on GD17 in the perichondrium of the proximal epiphysis. Further development of the innervation was characterized by the successive appearance of nerve fibres in the perichondrium/periosteum of the shaft (GD19), the bone marrow cavity and intercondylar eminence (GD21), the metaphyses (PD1), the cartilage canals penetrating into the epiphyses (PD7), and finally in the secondary ossification centres (PD10) and epiphyseal bone marrow (PD14). Maturation of the fibres, manifested by their immunoreactivity for CGRP and SP, was visible on GD21 in the epiphyseal perichondrium, the periosteum of the shaft and the bone marrow, on PD1 in the intercondylar eminence and the metaphyses, on PD7 in the cartilage canals, on PD10 in the secondary ossification centres and on PD14 in the epiphyseal bone marrow. The temporal and topographic pattern of nerve fibre appearance corresponds with the development of regions characterized by active mineralization and bone remodelling, suggesting a possible involvement of the sensory innervation in these processes.

Key words bone; fetus; immunohistochemistry; ossification.

Introduction

Early morphological studies applying classic histological methods, such as methylene blue staining and silver impregnation, revealed an intense innervation pattern of the bone in mature animals and humans (Kuntz & Richins, 1945; Miller & Kasahara, 1963; Thurston, 1982). More recent reports based on denervation experiments, retrograde tracing and immunohistochemistry have shown that those fibres belong to both afferent (sensory) and efferent (autonomic) populations (Bjurholm et al. 1988; Hill & Elde, 1991; Gajda et al. 2004). The majority of the skeletal innervation system is composed of sensory fibres originating from primary afferent neurons located in the dorsal root and some cranial nerve ganglia, whereas the other nerve fibre populations are adrenergic and cholinergic in nature and originate from paravertebral sympathetic ganglia. Being most numerous, sensory fibres were detected in the periosteum, bone marrow cavity and vascular canals in long bones of mature and developing animals (Bjurholm et al. 1988; Sisask et al. 1995; Mach et al. 2002).

Some early clinical reports suggest that peripheral innervation influences the development of bones and joints. Post-injectional sciatic nerve injury in neonates and children leads to a subnormal length growth of the long bones of the lower extremities (Gilles & French, 1961). Further experimental studies investigating the

Correspondence
Dr Mariusz Gajda, Department of Histology, Jagiellonian University, Medical College, Kopernika 7, 31-034 Kraków, Poland. T/F: +48 12 4227027; E: mmgajda@cyf-kr.edu.pl

Accepted for publication *29 April 2005*

influence of peripheral innervation on skeletal development, however, have yielded contradictory results in mammals. Most of these studies focused on the effect of peripheral denervation on limb development. Some authors did not find any effect (Gillespie, 1954), whereas others observed diminished (Edoff et al. 1997) or even increased growth of the denervated limb (Ring, 1961).

Divergent effects of denervation on the course of bone fracture repair, i.e. a process reflecting bone development (Ferguson et al. 1999), have been reported in both clinical investigations and experimental models. In experimentally denervated hindlimbs, the healing of fractured rat tibia was faster than in control animals (Aro et al. 1985). In a similar model of fractured and denervated tibia, however, extensive callus formation was detected radiographically (Nordsletten et al. 1994), but the mechanical properties of such a union were found to be significantly inferior compared with normal fracture healing (Madsen et al. 1998).

There is an increasing body of data suggesting that sensory terminals, in addition to an afferent role, may also act on the metabolism and proliferation of surrounding cells (Holzer, 1988). This trophic effect is believed to be mediated through the release of the neuropeptides calcitonin gene-related peptide (CGRP) and substance P (SP). Being widespread in sensory neurons and their processes, these peptides are commonly used as markers of sensory fibres in immunocytochemical studies (Bjurholm et al. 1988; Hill & Elde, 1991; Sisask et al. 1995; Hara-Irie et al. 1996).

Markers of growing nerve fibres are valuable in developmental investigations. The growth-associated protein 43 (GAP-43) is a cell membrane-bound protein present in developing and regenerating axons (for a review see Oestreicher et al. 1997), and has been successfully used in studies dealing with developmental bone innervation (Gajda et al. 2000). Protein gene product 9.5 (PGP 9.5) belongs to a group of ubiquitin hydrolases, is found in all populations of neurons and neuroendocrine cells, and has also been used in such investigations (Sisask et al. 1995, 1996).

To our knowledge, only a very limited number of papers have been published so far in which the authors have systematically followed the development of innervation in a long bone in the fetal and postnatal periods (Sisask et al. 1995, 1996; Gajda et al. 2000). Moreover, only Sisask et al. (1995, 1996) determined the chemical phenotype of these developing nerve fibres.

The aim of the present study was therefore to describe the time of appearance and topographical distribution of ingrowing sensory nerve fibres in developing bone. The tibia of rat hindlimbs was used as a model of the developing long bone, and an indirect double immunofluorescence method with antibodies against neuronal growth markers and sensory fibre-associated neuropeptides was applied for nerve fibre visualization.

Methods

Animals

Adult Wistar rats of both sexes and timed pregnant females were obtained from Charles River Laboratories (Brussels, Belgium). Conception was confirmed by the observation of the vaginal plug, referred as day 0 (GD0) of gestation (full gestation = 21 days). The animals were housed separately in acrylic cages with wood shavings in a climatized (22 ± 3 °C, 12/12-h dark–light cycle) room. They had unlimited access to water and standard rodent pellets. National and international principles of laboratory animal welfare (conforming to NIH publication 86-23, revised 1985) were followed and the experiments were approved by the local ethics committee of the University of Antwerp.

Pregnant rats were killed by an overdose of sodium pentobarbital (Nembutal, Sanofi, Belgium) administered intraperitoneally. Fetuses were obtained at gestational days (GD) 16 ($n = 8$ from two different mothers), GD17 ($n = 8$ from two different mothers), GD19 ($n = 8$ from two different mothers) and GD21 ($n = 8$ from two different mothers). The lower limbs of fetuses were dissected for further processing.

Offspring from different litters were killed at postnatal day (PD) 1 (day of birth; $n = 4$), PD2 ($n = 4$), PD3 ($n = 4$), PD4 ($n = 4$), PD7 ($n = 4$), PD10 ($n = 3$), PD14 ($n = 3$), PD21 ($n = 3$) and PD28 ($n = 4$) using an overdose of Nembutal. Hindlimbs were dissected and the skin was removed to allow better penetration of the fixative.

Deeply anaesthetized (as described above) animals older than PD7 were first transcardially perfused with cold Krebs–Ringer solution followed by 4% phosphate-buffered (0.1 M, pH = 7.4) freshly prepared paraformaldehyde; subsequently, limbs were postfixed as described below.

Tissue preparation

Dissected hindlimbs were fixed overnight by immersion in the paraformaldehyde solution at 4 °C, followed by

Table 1 Primary antibodies used in the study

Antigen (abbreviation)	Host/type	Dilution	Vendor; cat. number
Growth-associated protein 43 (GAP-43, GAP)	mouse/monoclonal	1 : 1000	Boehringer Mannheim, Mannheim, Germany; 1379011
Protein gene product 9.5 (PGP 9.5, PGP)	rabbit/polyclonal	1 : 500	Biogenesis, Poole, UK; 7863-0504
Calcitonin gene-related peptide (CGRP)	rabbit/polyclonal	1 : 500	Affiniti, Exeter, UK; CA1134
Substance P (SP)	rabbit/polyclonal	1 : 1000	Sigma, St. Louis, MO, USA; S-1542

rinsing in phosphate-buffered saline (PBS, 0.01 M, pH = 7.4). Hindlimbs from animals older than GD21 were decalcified in 10% EDTA in 0.1 M Tris buffer (pH = 7) at 4 °C for 5–14 days. The solution was refreshed every 2–3 days. The hindlimbs were then rinsed in PBS and immersed overnight in 25% sucrose in PBS with 0.01% sodium azide at 4 °C. Tissue blocks were mounted in TissueTek OCT compound (Sakura, Tokyo, Japan) on cryostat holders and rapidly frozen. Fifteen-micrometre-thick cryosections were cut in the sagittal plane, thaw-mounted on poly-L-lysine-coated slides and air-dried. Three to four serial sections were collected on each slide.

Immunohistochemistry

The procedures of material preparation that we used do not influence immunostaining (Bjurholm et al. 1989). A pre-incubation step with 10% normal goat serum in PBS containing 0.01% sodium azide, 0.05% thimerosal, 0.1% bovine serum albumin and 1% Triton X-100 was applied for 40 min to reduce non-specific binding and to increase penetration of the antibodies. For simultaneous demonstration of two antigens, an indirect double-staining immunofluorescence procedure was applied. The sections were incubated overnight at room temperature in humid chambers with mixtures of primary antibodies in the following combinations: GAP/PGP, GAP/CGRP and GAP/SP (see Table 1 for a list of the primary antisera used). After rinsing in PBS, sections were incubated for 2 h at room temperature with a mixture of biotinylated sheep anti-mouse serum (Amersham, Bucks., UK, RPN1001; diluted 1 : 200) and Cy3-conjugated goat anti-rabbit serum (Jackson IR, West Grove, PA, USA, 111-165-144; diluted 1 : 500). Following another rinse in PBS, FITC-conjugated streptavidin (Amersham, RPN1232; diluted 1 : 200) was applied for 1 h at room temperature. After a final rinse, the sections were mounted with Vectashield medium (Vector, Burlingame, CA, USA, H-1000) to minimize photobleaching of fluorochromes.

In the controls, the primary or secondary antibodies were omitted and replaced by non-immune serum.

Fluorescence microscopy

Sections were preliminarily examined under an Olympus BX-50 (Olympus, Tokyo, Japan) epifluorescence microscope equipped with filter sets: U-MNIBA and U-MNG for FITC and Cy3 visualization, respectively. For precise demonstration and co-localization of the examined antigens, the images were also registered with a Zeiss LSM 410 (Zeiss, Jena, Germany) confocal laser scanning microscope. An argon laser ($\lambda = 488$ nm), a helium–neon laser ($\lambda = 543$ nm) as well as appropriate dichroic mirrors and emission filters (FT510, LP515 and FT560, LP570) were used for excitation of the fluorochromes and acquisition of their emission spectra. Stacks of acquired optical sections were stored as graphic files and further processed with 3D-reconstruction software (Imaris 3.0, Bitplane AG, Zürich, Switzerland) working on an Indigo 2 station (Silicon Graphics, Mountain View, CA, USA). Final images were obtained as a result of 'extended focus/maximal intensity projection' transformation and presented as TIFF files at a resolution of 512×512 pixels.

Results

GAP-43 immunohistochemistry

In fetuses on GD16 GAP-43 immunoreactivity could not be observed in the close vicinity of the cartilaginous rudiment. However, it was present at this stage of development in thick nerve trunks as well as in nerve fibres located in the skin, in skeletal muscle and around large blood vessels. On GD17, the first few GAP-immunoreactive (IR) nerve fibres could be discerned in the perichondrium of the proximal epiphysis (Fig. 1) and, from GD19 onwards, in the perichondrium/periosteum of the diaphysis (Fig. 2). The number of perichondrial/

periosteal fibres clearly increased before birth (Fig. 4). They were located in both layers of the perichondrial and periosteal lining: thick fibres and nerve bundles were present in the superficial fibrous layer, and thin fibres and nerve terminals were seen in the deeper cellular lining (Fig. 5). The majority of these fibres were orientated parallel to the long axis of the rudiment.

From GD21 onwards, GAP-IR nerve fibres were observed in the osseous canals penetrating the interior of the bone and in the bone marrow cavity. Most of the fibres in the marrow were accompanying blood vessels (Figs 3 and 6), and non-vascular fibres were also occasionally seen running free between hemopoietic cells (Fig. 7). On PD1, some of the medullary fibres reached the proximal and distal metaphyses (Figs 6 and 8). From GD21 onwards, numerous nerve fibres were located in the region of the intercondylar eminence (Fig. 9).

GAP-immunopositive nerve fibres were present in the cartilage canals of the proximal and distal epiphyses from PD7 (Fig. 10), in the secondary ossification centre from PD10 (Fig. 11) and in the medullary spaces of both epiphyses from PD14, i.e. after formation of the growth plates.

After PD14, the distribution of GAP-IR nerve fibres did not change but the intensity of GAP-43 immunostaining was visibly diminished (Figs 3 and 12).

PGP 9.5 immunohistochemistry

The first few PGP-IR fibres were observed in the perichondrium of the proximal epiphysis at GD17 (Fig. 1), but the staining intensity was clearly weaker than that for GAP and for PGP in the later periods. From GD19, PGP-IR fibres were present in the diaphyseal perichondrium/periosteum (Fig. 2), and penetrated to the bone marrow cavity from GD21 (Fig. 3), reaching the metaphyseal regions around PD1. The number of fibres and intensity of PGP immunolabelling increased up to PD10 and then remained unchanged up to PD28. Immunopositive fibres were seen in the cartilage canals of both epiphyses from PD7 and in the secondary ossification centres from PD10. Co-localization of PGP and GAP was found up to PD28, although GAP-43 immunoreactivity was seen to decrease from PD14 onwards (Fig. 3).

CGRP and SP immunohistochemistry

The earliest CGRP-IR fibres were observed on GD21 in the perichondrium of both epiphyses (Fig. 4), the periosteum of the shaft (Fig. 5) and occasionally in the bone marrow cavity (Fig. 7). Perichondrial/periosteal fibres were located in both layers of the lining (Fig. 5). From PD1, they were also seen in the region of the intercondylar eminence (Fig. 9). Metaphyseal fibres (Figs 6 and 8) appeared around PD1. The number of CGRP-positive fibres was visibly increased on PD3. The majority of these fibres accompanied blood vessels, although free fibres were also observed.

The early CGRP-IR fibres fully co-localized with GAP, but $CGRP^{+}/GAP^{-}$ fibres were increasingly observed from PD1 onwards (Fig. 5).

CGRP-IR nerve fibres were seen in the cartilage canals of both epiphyses from PD7 (Fig. 10), in the secondary ossification centres from PD10 (Fig. 11) and in the bone marrow of the epiphyses from PD14. Some of these fibres were located along bone trabecules facing the growth plate (Fig. 12). The number and distribution of CGRP-IR fibres did not change after PD14. At the onset of secondary ossification centre formation, all related CGRP-IR fibres also expressed GAP, but from PD14 onwards numerous CGRP-IR fibres showed weak or no immunoreactivity for GAP in this area (Figs 10–12).

The sequence of appearance and localization of SP-IR fibres was similar to that of CGRP-containing fibres, except for the smaller number of fibres and weaker intensity of immunolabelling (data not shown). In contrast to GAP and PGP immunostaining, CGRP- and SP-IR labelling of fibres showed a characteristic, fine varicose appearance.

Discussion

The present study describes the time of appearance and localization of sensory nerve fibres in the developing long bone. The results obtained extend our current knowledge of long bone innervation during fetal and neonatal periods, especially as only a few reports have dealt with this problem so far (Calvo & Forteza-Vila, 1969; Calvo & Haas, 1969; Sisask et al. 1995, 1996; Hara-Irie et al. 1996; Gajda et al. 2000).

As expected, immunoreactivity for GAP-43 allowed the earliest possible visualization of nerve fibres in a developing bone (GD17), as GAP-43 is known to appear very early during axon formation and is necessary for its sprouting into target tissues (Oestreicher et al. 1997). GAP-43 was also the first marker to detect nerve fibres appearing in the area of bone fracture healing (Li et al. 2001). Other investigations successfully used GAP-43

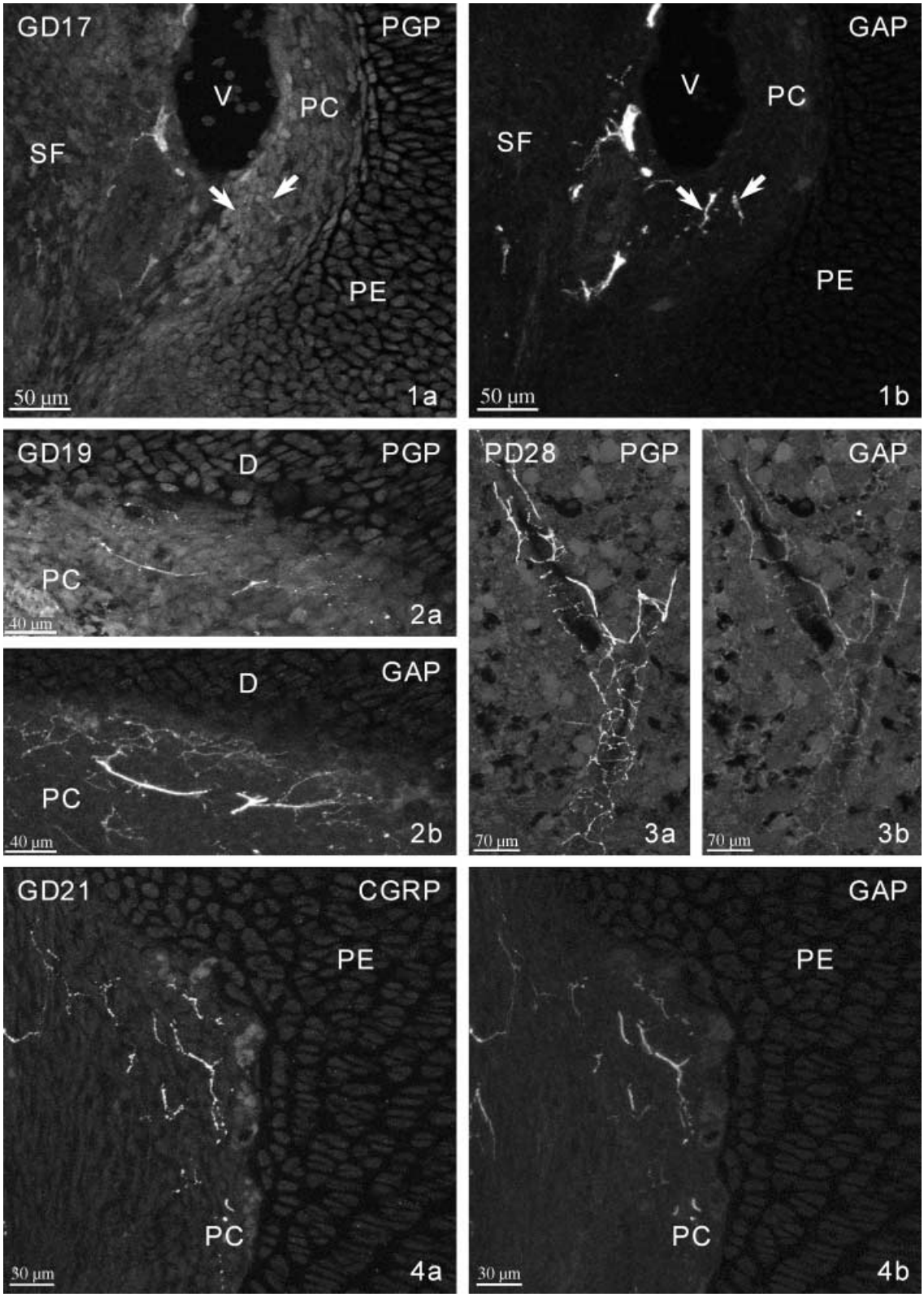

Fig. 1 GD17. PGP-immunonegative (a) and GAP-immunoreactive (IR) (b) fibres (arrows) in the perichondrium of the proximal epiphysis of the cartilagineous primordium. PE – proximal epiphysis, PC – perichondrium, V – vein, SF – subpopliteal fossa.
Fig. 2 GD19. PGP-IR (a) and GAP-IR (b) fibres in the perichondrium (PC) of the diaphysis (D).
Fig. 3 PD28. PGP-IR (a) and faintly GAP-IR (b) fibres accompanying a blood vessel in the bone marrow.
Fig. 4 GD21. CGRP-IR (a) and GAP-IR (b) fibres in the perichondrium (PC) of the proximal epiphysis (PE).

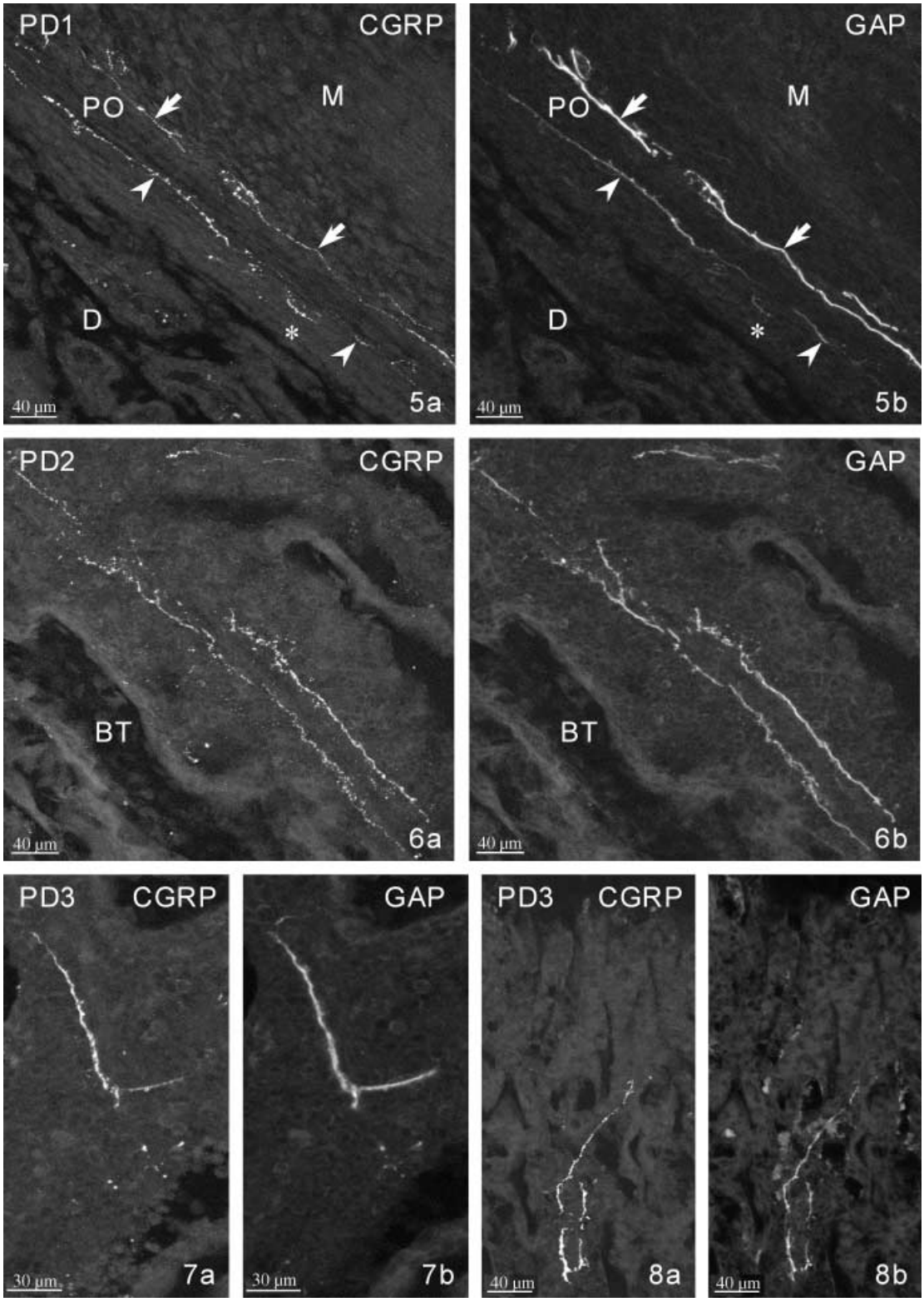

Fig. 5 PD1. CGRP-IR (a) and GAP-IR (b) fibres in the periosteum (PO) of the diaphysis: thick fibres and bundles in the outer fibrous layer (arrows), thin fibres and terminals in the deep cellular lining (arrowheads). Note some very weakly GAP-IR fibres in the inner layer (asterisk). PO – periosteum, D – diaphysis, M – skeletal muscles.

Fig. 6 PD2. CGRP-IR (a) and GAP-IR (b) fibres adjacent to a blood vessel in the bone marrow of the distal metaphysis. BT – bone trabecules.

Fig. 7 PD3. CGRP-IR (a) and GAP-IR (b) non-vascular fibres in the bone marrow of the central portion of the diaphysis.

Fig. 8 PD3. CGRP-IR (a) and GAP-IR (b) fibres in the bone marrow of the proximal metaphysis.

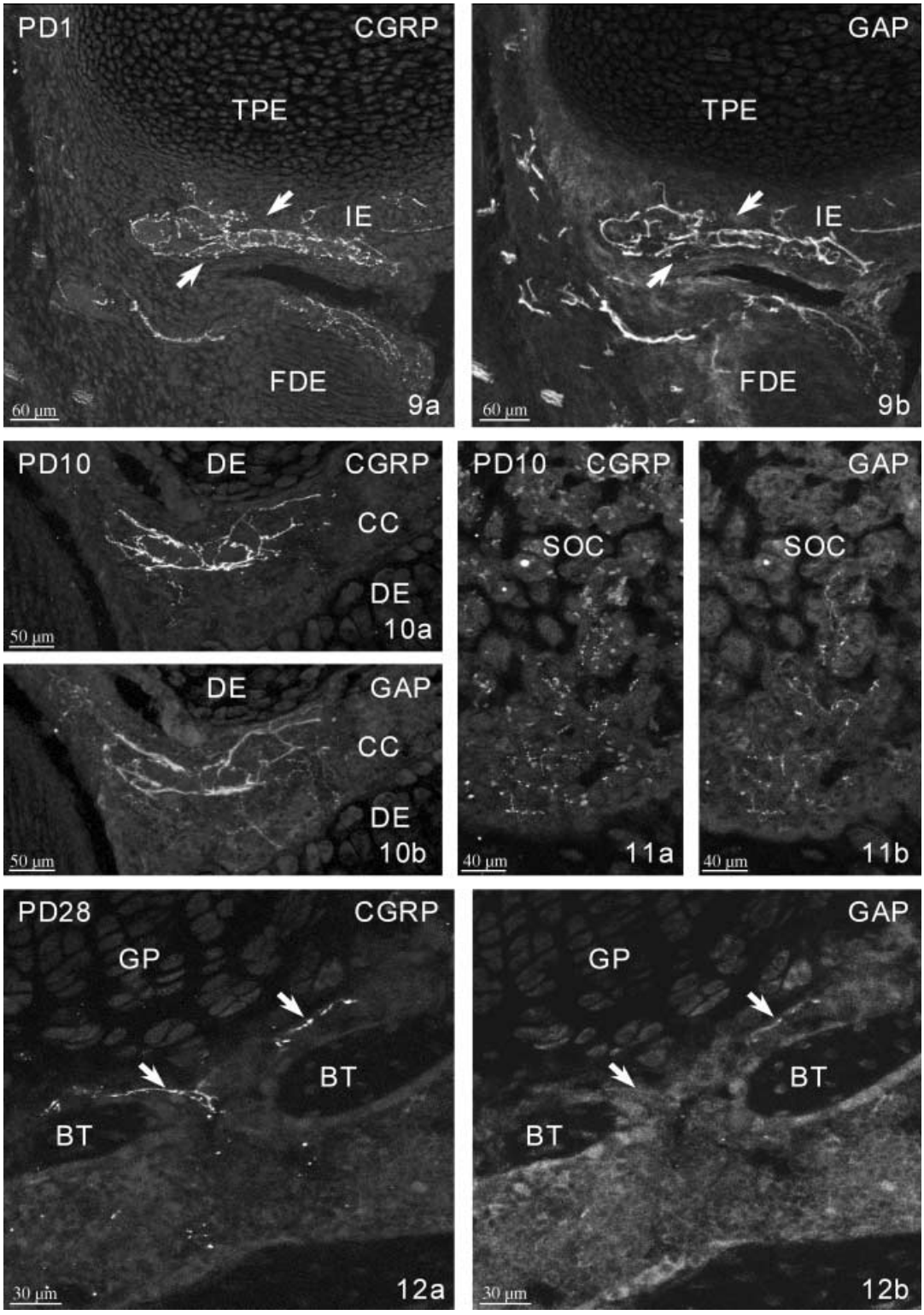

Fig. 9 PD1. CGRP-IR (a) and GAP-IR (b) fibres accompanying a blood vessel in the intercondylar eminence of the tibia (arrows). TPE – tibial proximal epiphysis, FDE – femoral distal epiphysis, IE – intercondylar eminence.
Fig. 10 PD10. CGRP-IR (a) and GAP-IR (b) vessel-associated fibres in the cartilage canal (CC) of the distal epiphysis. Note some negative or very weakly GAP-IR fibres.
Fig. 11 PD10. CGRP-IR (a) and GAP-IR (b) very fine fibres in the secondary ossification centre (SOC) of the proximal epiphysis.
Fig. 12 PD28. CGRP-IR (a) and GAP-negative or faintly GAP-IR (b) fibres (arrows) near the bone trabecules (BT) facing the growth plate (GP) in the proximal diaphysis.

for early identification of peripheral nerve fibres supplying different organs, such as taste buds (Mbiene & Mistretta, 1997) and pulmonary neuroepithelial bodies (Adriaensen et al. 2001), which require contact with nerve terminals for proper differentiation and further function.

The other neuronal marker applied in this study was PGP 9.5. Its presence in nerve fibres associated with tibial rudiment could also be observed from GD17 onwards, albeit that the initial intensity of immunostaining was much weaker than that of GAP-43. GAP-43 appears one day earlier (GD13) than PGP 9.5 (GD14) in nerve fibres of whole hindlimbs of rat fetuses (Jackman & Fitzgerald, 2000). In the studies of Sisask et al. (1995, 1996), it was PGP 9.5 that detected the earliest fibres (the authors did not study GAP-43). Hence, GAP-43 and PGP 9.5 may be considered as structural markers of fibres that are not yet chemically coded. They are present in all functional types of neurons and as such are non-selective pan-neuronal markers. The results of immunostaining for these proteins are similar to those obtained by using classical histological methods, such as silver impregnation (Calvo & Forteza-Vila, 1969; Thurston, 1982), methylene blue staining (Miller & Kasahara, 1963) and transmission electron microscopy (Calvo & Forteza-Vila, 1969; Hara-Irie et al. 1996; Imai et al. 1997). CGRP and SP expression appears later, i.e. on GD21. Double immunostaining revealed that GAP-43 fully co-localized with sensory markers at the early stages of development. From PD1 onwards, however, some sensory fibres lost GAP-43 expression and the number of such fibres increased with time as development-associated markers were replaced by those characteristic of the mature nerve fibres.

The earliest, very scanty nerve fibres around the tibial rudiment were found on GD17 in the perichondrium of the proximal epiphysis. More numerous perichondrial/periosteal fibres could be observed, predominantly around the diaphysis from GD19 onwards. Sisask et al. (1995, 1996) observed in previous studies on the development of bone innervation that the earliest nerve fibres related to bone rudiments of rat hindlimbs appeared as early as GD15. This discrepancy may arise from the anatomical location of the analysed bones. The latter authors investigated the primordia of all bones of the hindlimb, including the femur. The later appearance of innervation in our study may be explained by the more distal location of the tibia. Moreover, we adopted very strict topographical criteria, i.e. only fibres intimately related to the bone rudiment were considered.

In this study, the first CGRP- and SP-immunoreactive fibres in the tibial rudiment were found on GD21. The appearance of the neuromediator in nerve terminals is indicative of acquisition of final functional properties. Sisask et al. (1995) reported that the first sensory fibres containing CGRP and SP appeared slightly earlier in the developing rat femur, i.e. on GD19, concomitantly with the appearance of fibres expressing synaptophysin, a marker of active nerve terminals.

We observed an early appearance of nerve fibres in the bone marrow. In the present study, medullary fibres could be discerned as early as GD21, whereas Sisask et al. (1995, 1996) observed such fibres only from PD4 onwards. Our data are supported by results of Hara-Irie et al. (1996), who found CGRP-immunopositive fibres in the bone marrow cavity of the rat femur on GD19. An older report (Calvo & Haas, 1969) demonstrated nerve fibres visualized by silver impregnation in the bone marrow in late rat fetuses (GD21), still before blood cell precursors differentiated as members of the erythropoietic or myelopoietic families could be recognized.

A similar sequence of nerve fibre appearance has been observed in fracture healing and in ectopic bone formation. First, GAP-43-immunoreactive nerve fibres could be found in the fracture haematoma and periosteum as early as 3 days after experimental fracture of rat tibia (Li et al. 2001); PGP 9.5-immunoreactive fibres were present 1 week post-trauma and within 14 days CGRP-containing fibres were seen in the periosteum (Hukkanen et al. 1993). Three weeks after fracture, nerve fibres were found in the periosteum, in connective tissue and in the marrow spaces of the newly formed woven bone (Hukkanen et al. 1995). In rats, allogenic demineralized bone matrix implanted into the abdominal wall caused formation of cartilage 10 days after surgery, and 3 weeks after surgery a fully developed ossicle with bone marrow cavities could be observed (Bjurholm et al. 1990). Ten days after implantation, CGRP- and SP-immunoreactive fibres appeared in the connective tissue between chondroblast-like cells and after 3 weeks they are also seen in the bone marrow of the ossicle. CGRP-immunoreactive fibres appeared simultaneously with the mineralization of the implant (Bjurholm et al. 1990). The spatiotemporal pattern of nerve fibre appearance in fracture healing and ectopic bone formation, i.e. both processes involving mineralization of connective tissue and cartilage, is similar to that observed during long bone development.

There is a growing body of experimental data supporting the influence of sensory neuropeptides on the biology of bone cells during development. CGRP has been found to stimulate the proliferation of primary cultures of human osteoblasts (Villa et al. 2003) and to increase the number of osteoblastic bone colonies *in vitro* (Shih & Bernard, 1997a). Neurokinin receptors (NK1 and NK2) have also been demonstrated on osteoblasts (Fristad et al. 2003) and substance P has been found to cause an *in vitro* increase in the number and size of bone colonies (Shih & Bernard, 1997b). CGRP was shown to elevate cAMP (but not cGMP) level in cultured chondrocytes and perichondrial cells from rat pups (Edoff & Hildebrand, 2003). This effect was inhibited by CGRP1 receptor antagonist. Cartilage-projecting sensory neurons co-cultured with perichondrial cells expressed CGRP and SP, and they were depolarized by lowered pH (Edoff & Granseth, 2001). The action of CGRP is not only direct, because it also increases production of pro-osteogenic cytokines, such as insulin-like growth factor 1 and transforming growth factor β, by osteoblasts (Vignery & McCarthy, 1996; Wu et al. 2002).

Osteoclastic bone degradation is also influenced by sensory neuropeptides. A direct inhibition of osteoclastic activity by CGRP was documented by scanning electron microscopy (Zaidi et al. 1987). The total number of excavations as well as the total area of resorption on bone slices colonized by isolated rat neonatal osteoclasts were significantly lower in cultures maintained in the presence of CGRP. Electron microscopy revealed the presence of direct local contacts between non-myelinated nerve fibres and osteoclasts (Hara-Irie et al. 1996; Imai et al. 1997). Moreover, in denervated bones devoid of CGRP-immunoreactive fibres, osteoclasts displayed morphological features pointing to intense activity: a well-developed ruffled border, tight contact with the surface of the resorbed bone and increased activity of tartrate-resistant acid phosphatase (Hara-Irie et al. 1996). It seems plausible that neuropeptides released from sensory terminals promote new bone formation by stimulating osteoblasts and inhibiting osteoclasts.

Acknowledgements

Financial support was provided by a statutory grant 501/P/177/L from the Jagiellonian University, Medical College to J.A.L. We thank Danny Vindevogel for linguistic correction of the manuscript.

References

Adriaensen D, Scheuermann DW, Gajda M, Brouns I, Timmermans JP (2001) Functional implications of extensive new data on the innervation of pulmonary neuroepithelial bodies. *Ital J Anat Embryol* **106**, 395–403.

Aro H, Eerola E, Aho AJ (1985) Fracture healing in paraplegic rats. *Acta Orthop Scand* **56**, 228–232.

Bjurholm A, Kreicbergs A, Brodin E, Schultzberg M (1988) Substance P- and CGRP-immunoreactive nerves in bone. *Peptides* **9**, 165–171.

Bjurholm A, Kreicbergs A, Schultzberg M (1989) Fixation and demineralization of bone tissue for immunohistochemical staining of neuropeptides. *Calcif Tissue Int* **45**, 227–231.

Bjurholm A, Kreicbergs A, Dahlberg L, Schultzberg M (1990) The occurrence of neuropeptides at different stages of DBM-induced heterotopic bone formation. *Bone Miner* **10**, 95–107.

Calvo W, Forteza-Vila J (1969) On the development of bone marrow innervation in new-born rats as studied with silver impregnation and electron microscopy. *Am J Anat* **126**, 355–372.

Calvo W, Haas RJ (1969) Die Histogenese des Knochenmarks der Ratte: Nervale Versorgung, Knochenmarkstroma und ihre Beziehung zur Blutzellbildung [On the histogenesis of the bone marrow in the rat: innervation, stroma and their relations to hemopoiesis]. *Z Zellforsch Mikrosk Anat* **95**, 377–395.

Edoff K, Hellman J, Persliden J, Hildebrand C (1997) The developmental skeletal growth in the rat foot is reduced after denervation. *Anat Embryol* **195**, 531–538.

Edoff K, Granseth B (2001) Neuropeptide content and physiological properties of rat cartilage-projecting sensory neurones co-cultured with perichondrial cells. *Neurosci Lett* **315**, 141–144.

Edoff K, Hildebrand C (2003) Neuropeptide effects on rat chondrocytes and perichondrial cells *in vitro*. *Neuropeptides* **37**, 316–318.

Ferguson C, Alpern E, Miclau T, Helms JA (1999) Does adult fracture repair recapitulate embryonic skeletal formation? *Mech Dev* **87**, 57–66.

Fristad I, Vandevska-Radunovic V, Fjeld K, Wimalawansa SJ, Hals K, I (2003) NK1, NK2, NK3 and CGRP1 receptors identified in rat oral soft tissues, and in bone and dental hard tissue cells. *Cell Tissue Res* **311**, 383–391.

Gajda M, Adriaensen D, Cichocki T (2000) Development of the innervation of long bones: expression of the growth-associated protein 43. *Folia Histochem Cytobiol* **38**, 103–110.

Gajda M, Litwin JA, Adriaensen D, Timmermans JP, Cichocki T (2004) Segmental distribution and morphometric features of primary sensory neurons projecting to the tibial periosteum in the rat. *Folia Histochem Cytobiol* **42**, 95–99.

Gilles FH, French JH (1961) Postinjection sciatic nerve palsies in infants and children. *J Pediatr* **58**, 195–204.

Gillespie JA (1954) The nature of the bone changes associated with nerve injuries and disuse. *J Bone Joint Surg Br* **36**, 464–473.

Hara-Irie F, Amizuka N, Ozawa H (1996) Immunohistochemical and ultrastructural localization of CGRP-positive nerve fibers at the epiphyseal trabecules facing the growth plate of rat femurs. *Bone* **18**, 29–39.

Hill EL, Elde R (1991) Distribution of CGRP-, VIP-, DβH-, SP-, and NPY-immunoreactive nerves in the periosteum of the rat. *Cell Tissue Res* **264**, 469–480.

Holzer P (1988) Local effector functions of capsaicin-sensitive sensory nerve endings: involvement of tachykinins, calcitonin gene-related peptide and other neuropeptides. *Neuroscience* **24**, 739–768.

Hukkanen M, Konttinen YT, Santavirta S, et al. (1993) Rapid proliferation of calcitonin gene-related peptide-immunoreactive nerves during healing of rat tibial fracture suggests neural involvement in bone growth and remodelling. *Neuroscience* **54**, 969–979.

Hukkanen M, Konttinen YT, Santavirta S, et al. (1995) Effect of sciatic nerve section on neural ingrowth into the rat tibial fracture callus. *Clin Orthop* **311**, 247–257.

Imai S, Rauvala H, Konttinen YT, et al. (1997) Efferent targets of osseous CGRP-immunoreactive nerve fiber before and after bone destruction in adjuvant arthritic rat: an ultramorphological study on their terminal-target relations. *J Bone Miner Res* **12**, 1018–1027.

Jackman A, Fitzgerald M (2000) Development of peripheral hindlimb and central spinal cord innervation by subpopulations of dorsal root ganglion cells in the embryonic rat. *J Comp Neurol* **418**, 281–298.

Kuntz A, Richins CA (1945) Innervation of the bone marrow. *J Comp Neurol* **83**, 213–221.

Li J, Ahmad T, Spetea M, Ahmed M, Kreicbergs A (2001) Bone reinnervation after fracture: a study in the rat. *J Bone Miner Res* **16**, 1505–1510.

Mach DB, Rogers SD, Sabino MC, et al. (2002) Origins of skeletal pain: sensory and sympathetic innervation of the mouse femur. *Neuroscience* **113**, 155–166.

Madsen JE, Hukkanen M, Aune AK, et al. (1998) Fracture healing and callus innervation after peripheral nerve resection in rats. *Clin Orthop* **351**, 230–240.

Mbiene JP, Mistretta CM (1997) Initial innervation of embryonic rat tongue and developing taste papillae: nerves follow distinctive and spatially restricted pathways. *Acta Anat* **160**, 139–158.

Miller MR, Kasahara M (1963) Observations on the innervation of human long bones. *Anat Rec* **145**, 13–23.

Nordsletten L, Madsen JE, Almaas R, et al. (1994) The neuronal regulation of fracture healing. Effects of sciatic nerve resection in rat tibia. *Acta Orthop Scand* **65**, 299–304.

Oestreicher AB, De Graan PN, Gispen WH, Verhaagen J, Schrama LH (1997) B-50, the growth associated protein-43: modulation of cell morphology and communication in the nervous system. *Prog Neurobiol* **53**, 627–686.

Ring PA (1961) The influence of the nervous system upon the growth of bones. *J Bone Joint Surg Br* **43**, 121–140.

Shih C, Bernard GW (1997a) Calcitonin gene related peptide enhances bone colony development in vitro. *Clin Orthop* **334**, 335–344.

Shih C, Bernard GW (1997b) Neurogenic substance P stimulates osteogenesis in vitro. *Peptides* **18**, 323–326.

Sisask G, Bjurholm A, Ahmed M, Kreicbergs A (1995) Ontogeny of sensory nerves in the developing skeleton. *Anat Rec* **243**, 234–240.

Sisask G, Bjurholm A, Ahmed M, Kreicbergs A (1996) The development of autonomic innervation in bone and joints of the rat. *J Auton Nerv Syst* **59**, 27–33.

Thurston TJ (1982) Distribution of nerves in long bones as shown by silver impregnation. *J Anat* **134**, 719–728.

Vignery A, McCarthy TL (1996) The neuropeptide calcitonin gene-related peptide stimulates insulin-like growth factor I production by primary fetal rat osteoblasts. *Bone* **18**, 331–335.

Villa I, Dal Fiume C, Maestroni A, Rubinacci A, Ravasi F, Guidobono F (2003) Human osteoblast-like cell proliferation induced by calcitonin-related peptides involves PKC activity. *Am J Physiol Endocrinol Metab* **284**, E627–E633.

Wu Z, Nagata K, Iijima T (2002) Involvement of sensory nerves and immune cells in osteophyte formation in the ankle joint of adjuvant arthritic rats. *Histochem Cell Biol* **118**, 213–220.

Zaidi M, Fuller K, Bevis PJ, Gaines Das RE, Chambers TJ, MacIntyre I (1987) Calcitonin gene-related peptide inhibits osteoclastic bone resorption: a comparative study. *Calcif Tissue Int* **40**, 149–154.